LETTERS

Twinning superlattices in indium phosphide nanowires

Rienk E. Algra[1,2,3], Marcel A. Verheijen[2], Magnus T. Borgström[2]†, Lou-Fé Feiner[2], George Immink[2], Willem J. P. van Enckevort[3], Elias Vlieg[3] & Erik P. A. M. Bakkers[2]

Semiconducting nanowires offer the possibility of nearly unlimited complex bottom-up design[1,2], which allows for new device concepts[3,4]. However, essential parameters that determine the electronic quality of the wires, and which have not been controlled yet for the III–V compound semiconductors, are the wire crystal structure and the stacking fault density[5]. In addition, a significant feature would be to have a constant spacing between rotational twins in the wires such that a twinning superlattice is formed, as this is predicted to induce a direct bandgap in normally indirect bandgap semiconductors[6,7], such as silicon and gallium phosphide. Optically active versions of these technologically relevant semiconductors could have a significant impact on the electronics[8] and optics[9] industry. Here we show first that we can control the crystal structure of indium phosphide (InP) nanowires by using impurity dopants. We have found that zinc decreases the activation barrier for two-dimensional nucleation growth of zinc-blende InP and therefore promotes crystallization of the InP nanowires in the zinc-blende, instead of the commonly found wurtzite, crystal structure[10]. More importantly, we then demonstrate that we can, once we have enforced the zinc-blende crystal structure, induce twinning superlattices with long-range order in InP nanowires. We can tune the spacing of the superlattices by changing the wire diameter and the zinc concentration, and we present a model based on the distortion of the catalyst droplet in response to the evolution of the cross-sectional shape of the nanowires to quantitatively explain the formation of the periodic twinning.

Twin planes and, more generally, planar stacking faults are commonly found in III–V nanowires grown in the [111] direction by the vapour-liquid-solid (VLS) mechanism. A twin plane in a zinc-blende (stacking fault in a wurtzite) nanowire can be considered as a monolayer of the wurtzite (zinc blende) phase[11]. Stacking faults can significantly affect the electronic properties of the nanowires[5,7]. The electron wavefunction is discontinuous at a stacking fault, which leads, for instance, to a reduced mobility of charge carriers. The formation and resulting morphology of randomly distributed stacking faults in nanowires have been investigated by several authors[11–14]. Twin planes that have a constant spacing within a nanowire form a twinning superlattice (TSL); this modifies the electronic band structure, giving rise to the formation of minibands[7]. Recently, small domain TSLs have been observed locally in bulk Si[15,16], and occasionally in ZnS nanowires[17], but the parameters controlling the phenomenon were not identified.

The first step in obtaining a TSL is to control the nanowire crystal structure. Bulk InP has the zinc-blende crystal structure, because the free energy is slightly lower ($\Delta E = 6.8$ meV per III–V atom pair)[18] for this structure than for InP with the wurtzite structure. However, nominally undoped InP nanowires commonly exhibit the wurtzite crystal structure. Possible explanations for the formation of wurtzite nanowires are the lower surface energy of the parallel side facets of wurtzite wires compared to that of zinc-blende wires[18] and the interface energies at the vapour–liquid–solid three-phase line[19]. These effects would make crystallization in the wurtzite phase especially favourable for thin wires that have a large surface to bulk ratio.

We have synthesized InP nanowires from colloidal gold particles by VLS growth using metal-organic vapour phase epitaxy (MOVPE) with trimethylindium and phosphine as molecular precursors (Methods Summary). We consistently observe that undoped InP wires (with diameters of 10–250 nm) have the wurtzite structure, though in general contain many stacking faults. With increasing diameter the number of stacking faults decreases, leading to wires with a larger fraction of wurtzite structure and showing that the above-mentioned factors do not ultimately determine the crystal structure of the wires.

The main difference between bulk and VLS growth is the presence of the catalyst particle from which the crystal is precipitated, and therefore the atomic interactions at the liquid–solid interface should be considered. We find that the parameter critically determining the nanowire crystal structure and the stacking fault density is the chemical composition of the catalyst particle near the liquid–solid interface. We introduce diethylzinc in the growth system to establish p-type doping in our nanowires. Importantly, when sufficient Zn is added to the system, the nanowires precipitate in the zinc-blende crystal structure. We find a transition from wurtzite to zinc-blende structure at a diethylzinc partial pressure of 4.6×10^{-5} mbar (4.6×10^{-4} mbar corresponds to a free hole concentration of 10^{18} cm^{-3} in the InP nanowires[20]), as is shown in Fig. 1a (see also Supplementary Information 1). For diethylzinc partial pressures between 4.6×10^{-5} and 4.6×10^{-4} mbar, we find that twin planes are randomly distributed in the nanowires. Strikingly, above 4.6×10^{-4} mbar, the twin planes exhibit a constant spacing for a given Zn concentration and wire diameter, and the nanowire develops a TSL. The segment length of the TSL increases with the Zn concentration.

To quantify the effect of Zn on the crystal structure, we have calculated, based on two-dimensional nucleation, a kinetic phase diagram (Fig. 1b). The obtained curve, which relates the supersaturation in the droplet, $\Delta\mu$, to the (normalized) difference in solid–liquid step free energy between a zinc-blende and a wurtzite nucleus, $\Delta\gamma/\gamma_{sl,ZB}$, separates the domains of wurtzite and zinc-blende nanowire growth (see Supplementary Information 2). As elaborated in the Supplementary Information, we argue that the main effect of adding zinc during growth is a decrease in $\Delta\gamma/\gamma_{sl,ZB}$, which means a lowering of the liquid–solid step energy for zinc blende as compared to wurtzite. This suggests a strong interaction of the zinc atoms with the InP

[1]Materials Innovation Institute (M2i), 2628CD Delft, The Netherlands. [2]Philips Research Laboratories Eindhoven, High Tech Campus 11, 5656AE Eindhoven, The Netherlands. [3]IMM, Solid State Chemistry, Radboud University Nijmegen, Heijendaalseweg 135, 6525AJ Nijmegen, The Netherlands. †Present address: Solid State Physics, Lund University, Box 118, S-221 00 Lund, Sweden.

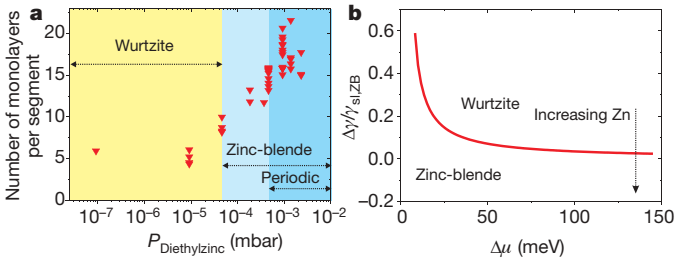

Figure 1 | The effect of Zn-doping on the InP nanowire crystal structure. **a**, The average segment length (number of monolayers, ML, per segment) between two adjacent stacking faults or twin planes as a function of the diethylzinc concentration. A transition from the wurtzite to the zinc-blende crystal structure is observed at 4.6×10^{-5} mbar diethylzinc, and above 4.6×10^{-4} mbar the twin planes are periodic for a given dopant level. The data refer to wires with diameters between 15 and 25 nm. **b**, Calculated kinetic phase diagram showing the domains of wurtzite and zinc blende as a function of $\Delta\gamma/\gamma_{sl,ZB}$ and $\Delta\mu$. Zn reduces the liquid–solid step energy of the zinc-blende structure with respect to the wurtzite structure and thus promotes the formation of zinc-blende-structured InP wires.

growth interface, as was also observed during electrical resistance measurements of Au(Zn)–InP contacts[21,22]. In general, for nanowires grown by the VLS mechanism, the crystal structure may be intrinsically different from that of the bulk material and will depend on the combination of semiconductor with catalyst material.

Having adequate control over the nanowire crystal structure, we can now address the formation of TSLs. In Fig. 2, images from transmission electron microscopy (TEM) are shown of Zn-doped (9.2×10^{-4} mbar) InP nanowires with nominal diameters of 10, 20, 50 and 100 nm. It is clear from the overview images in Fig. 2a that the periodically twinned structure is general, although not all of the wires have the optimal orientation with respect to the electron beam. The segment length is uniform (Fig. 2b) throughout the wires. From the high resolution images in Fig. 2c, we observe that the periodic nanowires have the zinc-blende crystal structure with {111} side facets, which are not parallel with respect to the long nanowire axis. Using the high resolution images, the number of monolayers between successive twin planes was counted, and the data are plotted in the histograms shown in Fig. 3a (here, a monolayer with thickness $d_{111} = 3.4$ Å contains pairs of In and P atoms). Segment lengths of 7 ± 2, 13 ± 2, 25 ± 3 and 33 ± 6 monolayers were found for wires with a diameter of 10, 20, 50 and 100 nm, respectively (Fig. 3a). Importantly, the periodicity in twinning is demonstrated by the relatively narrow distributions in segment lengths.

For the formation of the TSL, it is crucial that the {111}A and {111}B side facets are tilted in opposite directions (by $\theta = \theta_B = -\theta_A \approx 19.5^\circ$) with respect to the nanowire axis (Fig. 2c). As shown schematically in Fig. 4, at a certain moment during growth (situations 1 and 3) the top surface of the nanowire is a hexagon, and the shape of the catalyst droplet, connected to this surface, is close to spherical. When the wire grows, the {111}A edges move inward and their length increases, while the {111}B edges move outward and their length decreases. Thus the shape of the nanowire–droplet interface becomes increasingly triangle-like, as shown for situations 2 and 4 in Fig. 4b. This induces the catalyst droplet to distort so as to minimize its surface area, leaning over towards the long {111}A edges. At a certain point it becomes more favourable to form a twin plane and to start reducing the distortion of the catalyst particle by re-growth towards a hexagonal shape, rather than to continue growth towards a completely triangular shape. This mechanism of inverting triangularly shaped interfaces repeats itself continuously and produces the periodically structured wire.

To understand this process in more detail, we developed a quantitative model based on a specific mechanism relating the distortion of the droplet to the growth process (details are given in Supplementary Information 3). Nanowire growth proceeds layer by layer with a single nucleation event per layer, initiated at the nanowire edge[12]. The free energy of formation of the nucleus depends on the difference between the liquid–solid contact angle and the tilt angle of the external facet of the nucleus. We have analysed this dependence quantitatively, making use of the simulator program Surface Evolver[23,24]. It follows that the formation of nuclei with an external

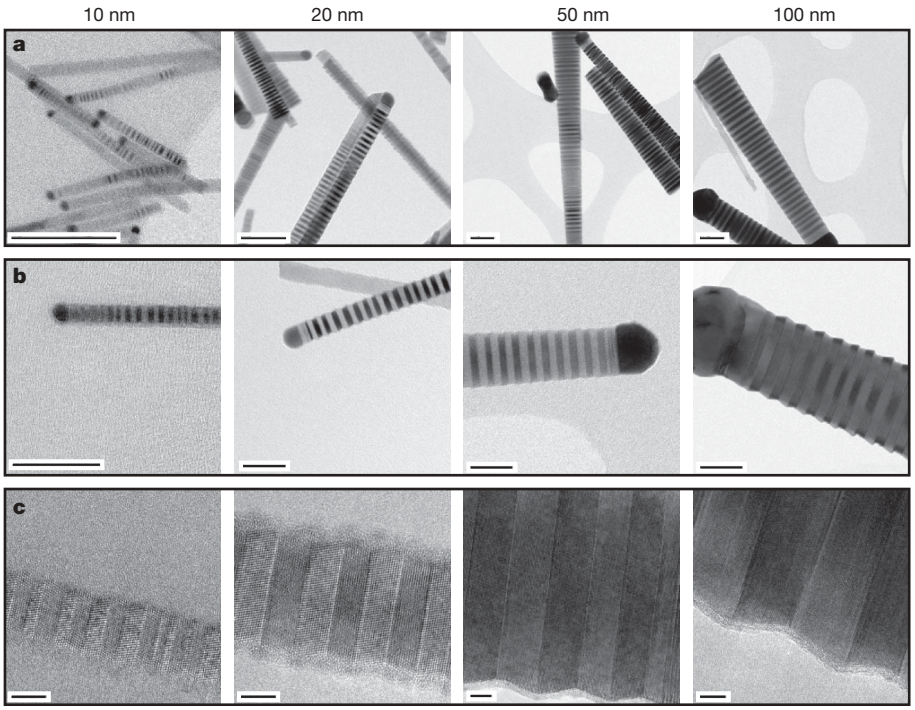

Figure 2 | TEM images of nanowire TSLs. **a**–**c**, Overview (**a**, **b**) and high resolution (**c**) TEM images of InP nanowires with a diameter of nominally 10, 20, 50 and 100 nm (columns 1–4, left to right) and a diethylzinc partial pressure of 9.7×10^{-4} mbar. Scale bars: **a**, 100 nm; **b**, 50 nm; and **c**, 5 nm. The images are all taken close to the catalyst particle and therefore the observed side facets are due to the VLS growth. Lateral growth is also observed further down the nanowire.

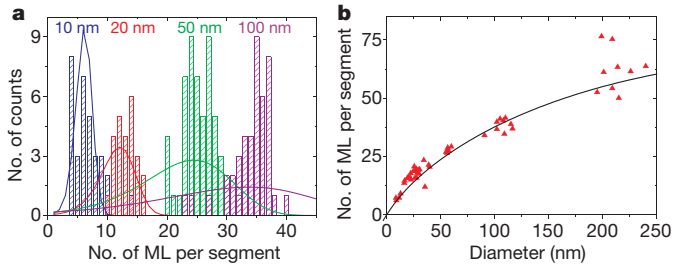

Figure 3 | The effect of wire diameter on the twin lattice spacing. **a**, Histograms of the number of monolayers (ML) between two consecutive twin planes for wires with a nominal diameter of 10, 20, 50 and 100 nm. The narrow distributions demonstrate the periodicity. The curves give the calculated distributions obtained from the quantitative model, using the same parameter values as in **b**. **b**, The number of monolayers per segment versus the diameter. Each data point represents an averaged value of 25–50 segments, taken from a single nanowire with 9.7×10^{-4} mbar diethylzinc doping. The curve is the theoretical expression given in the text, with $\Delta = 4.5$ and $N_c = AD$ with $A = 0.35\,\mathrm{nm}^{-1}$.

(solid–vapour) A-facet is strongly suppressed. As a result, the dominant processes are nucleation of external-B-facet nuclei at either B edges, adding another facet-conserving zinc-blende layer, or at A edges, introducing a layer that involves a twin plane and initiating re-growth. During facet-conserving growth, the liquid–solid contact angles increase (decrease) at the A edges (B edges) owing to the progressing droplet distortion illustrated in Fig. 4.

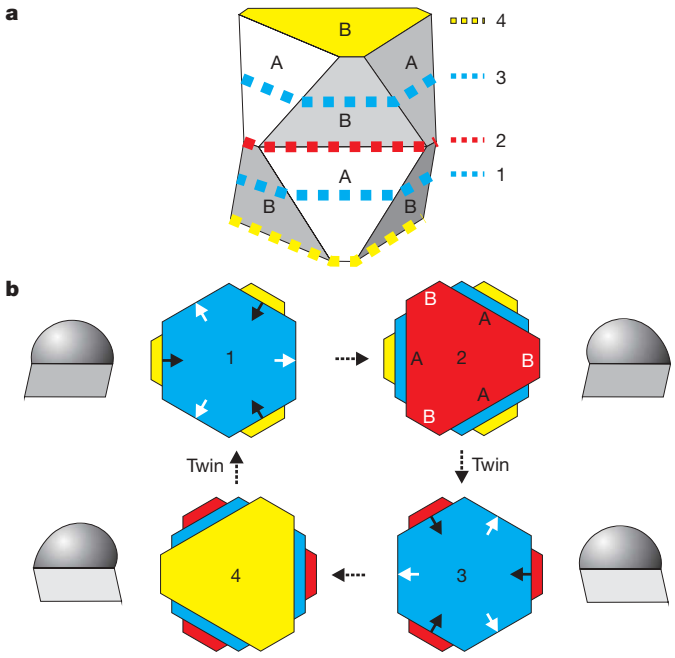

Figure 4 | Model for periodic twinning in nanowires. **a**, Schematic representation of the morphology of a twinned nanowire with the zinc-blende crystal structure with non-parallel {111} side facets. **b**, The cross-sectional shapes of the top facet of the nanowire crystal at the solid–liquid interface during growth. The numbers correspond to the positions indicated in **a**. Owing to the non-parallel orientation of the side facets, {111}A edges increase and {111}B edges decrease in length during vertical growth, and as a result a hexagonal interface develops into a triangle-like shape. At a certain moment, it is energetically more favourable to create a twin plane rather than to continue growing towards a fully triangular top interface. After twin formation, a triangle-like shape evolves back to a hexagonal shape and the cycle is repeated as schematized in **b**. To the left or right the corresponding calculated shape of the catalyst particle on a hexagonal (1 and 3) and a triangularly deformed (2 and 4) interface is depicted, showing the skewing of the droplet towards the long {111}A side edge and demonstrating that the contact angles depend sensitively on the cross-sectional shape.

We find that the contact angles depend linearly on the ratio of the wire height $H = Nh$ (with N the number of monolayers measured from the last hexagonal cross-section, and h the layer thickness) and the wire diameter D. This is similar to what has been observed for sawtooth faceting in Si nanowires and tentatively explained by considerations based on total energies instead of nucleation energies[25]. From this, it follows that the difference in free energy of the two competing nucleation processes, $\delta\Delta G^*$, decreases linearly with wire height as $\delta\Delta G^* = \delta\Delta G_0^* - CNh/D$, where $\delta\Delta G_0^*$ is the free energy difference at hexagonal interface shape and C is a constant with the dimension of energy. As a result, we find that the critical number of monolayers, N_c, at which twin formation becomes the more favourable process, is proportional to the wire diameter D. However, the segment length will be substantially less than $2N_c$, because it is determined by the probability of an uninterrupted series of facet-conserving nucleations followed by a facet-changing nucleation. Taking this statistical aspect into account, we find that the number of layers in a segment is given by $N_s = 2N_c(1 + (1/\Delta)\ln[1 - \exp(-\Delta/N_c)])$, where $\Delta = \delta\Delta G_0^*/k_B T$ (here k_B is the Boltzmann constant and T is temperature). We find excellent agreement between this expression and the observed diameter dependence (Fig. 3b), if we make use of the explicit expressions (see Supplementary Information 3, and L.-F.F., manuscript in preparation) for $\delta\Delta G_0^*$ and N_c in terms of the physical parameters. These parameters are the solid–liquid surface tension γ_{SL}, liquid–vapour surface tension γ_{LV}, surface energy of a twin plane γ_T, supersaturation $\Delta\mu$, tilting angle θ, contact angle at hexagonal interface shape β_0, and temperature T. In Fig. 3 we used $T = 713\,\mathrm{K}$, $\gamma_T = 0.009\,\mathrm{J\,m^{-2}}$ (refs 18, 26), $\gamma_{SL} \approx \gamma_{SV} \approx 0.8\,\mathrm{J\,m^{-2}}$ (ref. 27), $\gamma_{LV} = 1.0\,\mathrm{J\,m^{-2}}$ (in between the values for liquid Au and In), with $\beta_0 \approx 98^\circ$, and $\Delta\mu = 180\,\mathrm{meV}$ per atom pair, which are physically plausible values.

In addition, the statistical analysis yields the width of the segment length distribution (Fig. 3a), using the same parameter values. The trend of increasing width with diameter is correctly reproduced, but the effect is overestimated for the thicker wires. This cannot solely be explained by the probably slightly smaller supersaturation for the larger-diameter nanowires, and could indicate that other energies or effects not included in the model might play a role here.

In general, to obtain a nanowire TSL with a narrow segment distribution, a large $\delta\Delta G_0^*$ and fairly small N_c are required. As $\delta\Delta G_0^*$ depends on supersaturation as $\delta\Delta G_0^* \propto (1/\Delta\mu)^2$, and N_c on supersaturation and wire diameter as $N_c \propto D/\Delta\mu$, it is clear that the supersaturation, determined by the trimethylindium flow, should be chosen low in order to increase $\delta\Delta G_0^*$, and the accompanying increase of N_c be compensated by having a small wire diameter, determined by the catalyst size.

Taking the above design rules into consideration, we have recently obtained a TSL structure in Zn-doped GaP nanowires, albeit with a broader segment length distribution. This preliminary result from a different materials system substantiates the general nature of the present approach.

Our insight into the formation of twins allows the fabrication of more complex structures by varying the Zn concentration during growth. Without Zn, random stacking faults in a wurtzite crystal structure should occur, and with Zn present the twinning should become periodic. This is indeed the case, as demonstrated by the TEM images in Fig. 5a and b, showing a wire for which a diethylzinc partial pressure of 9.2×10^{-4} mbar has been used intermittently during growth. The tapering of the nanowire is due to sidewall growth, which preferentially occurs on the zinc-blende sections. In Fig. 5c, the length of the zinc-blende sections has been plotted against the time interval during which the Zn precursor gas flow was switched on. The fitted linear curve has an insignificant offset from zero, suggesting an almost immediate switching from the wurtzite to the zinc-blende phase and vice versa. In Fig. 5d the number of monolayers between two twin planes is presented for the first four zinc-blende sections. The average segment length is 13 ± 3 monolayers,

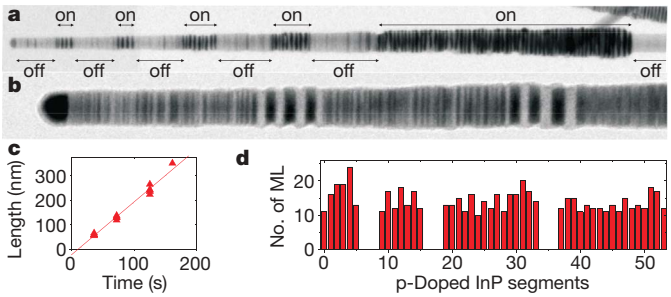

Figure 5 | InP nanowire with alternating periodic and non-periodic segments. a, An overview TEM image of a wire containing segments of intrinsic InP (containing randomly distributed stacking faults in a wurtzite structure) and Zn doped (9.7×10^{-4} mbar) segments (with different lengths) with periodic twin planes in a zinc-blende structure. The 'on' represents the p-doped segments where diethylzinc is added, whereas the 'off' represents the intrinsic, undoped, segments. **b**, Higher magnification TEM image of the segments closest to the gold particle. **c**, Zinc-blende section length versus the time interval during which the diethylzinc precursor gas flow was switched on. The intercept at approximately zero shows abrupt switching between the zinc-blende and wurtzite crystal structure. **d**, Number of monolayers between two successive twin planes in each p-doped segment obtained from HRTEM. An average of $\sim 13 \pm 3$ monolayers is found.

showing that the periodicity is clearly preserved in these short sections and is not affected by the growth history.

We have presented a viable and general route for the fabrication of TSLs in nanowires by controlling the nanowire morphology. This new instrument for manipulating the electronic properties of nanowires can be combined with already demonstrated features such as axial and radial heterostructures and doping profiles, further expanding the nanowire toolbox.

METHODS SUMMARY

The InP nanowires were synthesized in a low pressure (50 mbar) Aixtron 200 MOVPE reactor on InP (111)B substrates. The substrates were treated with a piranha etch for 1 min to remove the surface oxide, before deposition of Au colloids of different diameters (ranging from 10 to 200 nm). The nanowires were grown in the VLS growth mode using trimethylindium and phosphine as precursors, at partial pressures of 1.19×10^{-3} and 4.17×10^{-1} mbar, respectively, in a total flow of 6 l min^{-1} hydrogen carrier gas. As dopant material diethylzinc was used for p-type doping. Before growth, an anneal step was carried out under phosphine/hydrogen atmosphere to desorb any surface oxide and to alloy the Au colloids with the InP substrate to ensure epitaxial growth. Growth was initiated when a temperature of 420 °C was reached by switching on the trimethylindium. To change the dopant concentrations in the wires, the diethylzinc partial pressure was varied between 10^{-2} and 10^{-7} mbar, at constant trimethylindium and phosphine molar fractions in hydrogen. We point out that the molar fractions given for diethylzinc are those in the controlled gas flows in the reactor and not necessarily the built-in atomic fractions in the wires. The samples were analysed using TEM (FEI Tecnai 300 kV) in bright field, and high resolution TEM.

Received 8 April; accepted 16 October 2008.

1. Gudikson, M. S. *et al.* Growth of nanowire superlattice structures for nanoscale photonics and electronics. *Nature* **415,** 617–620 (2002).
2. Dick, K. A. *et al.* Synthesis of branched 'nanotrees' by controlled seeding of multiple branching events. *Nature Mater.* **3,** 380–384 (2004).
3. Hochbaum, A. I. *et al.* Enhanced thermoelectric performance of rough silicon nanowires. *Nature* **451,** 163–168 (2008).
4. van Dam, J. A. *et al.* Supercurrent reversal in quantum dots. *Nature* **442,** 667–670 (2006).
5. Bao, J. *et al.* Optical properties of rotationally twinned InP nanowire heterostructures. *Nano Lett.* **8,** 836–841 (2008).
6. Ikonic, Z. *et al.* Electronic properties of twin boundaries and twinning superlattices in diamond-type and zinc-blende-type semiconductors. *Phys. Rev. B* **48,** 17181–17193 (1993).
7. Ikonic, Z. *et al.* Optical properties of twinning superlattices in diamond-type and zinc-blende-type semiconductors. *Phys. Rev. B* **52,** 14078–14085 (1995).
8. Lui, A. S. *et al.* Advances in silicon photonic devices for silicon based optoelectronic applications. *Physica E* **35,** 223–228 (2006).
9. Krames, M. R. *et al.* Status and future of high-power light-emitting diodes for solid-state lighting. *J. Display Tech.* **3,** 160–175 (2007).
10. Mattila, M. *et al.* Crystal-structure-dependent photoluminescence from InP nanowires. *Nanotechnology* **17,** 1580–1583 (2006).
11. Hiruma, K. *et al.* Growth and optical properties of nanometer scale GaAs and InAs whiskers. *J. Appl. Phys.* **77,** 447–462 (1995).
12. Johansson, J. *et al.* Structural properties of <111>B-oriented III–V nanowires. *Nature Mater.* **5,** 574–580 (2006).
13. Xiong, Q. *et al.* Coherent twinning phenomena: Towards twinning superlattices in III–V semiconducting nanowires. *Nano Lett.* **6,** 2736–2742 (2006).
14. Verheijen, M. A. *et al.* Three dimensional morphology of GaP-GaAs nanowires revealed by transmission electron microscopy tomography. *Nano Lett.* **7,** 3051–3055 (2007).
15. Fissel, A. *et al.* Formation of twinning-superlattice regions by artificial stacking of Si layers. *J. Cryst. Growth* **290,** 392–397 (2006).
16. Hibino, H. *et al.* Twinned epitaxial layers formed on Si(111) $\sqrt{3}\times\sqrt{3}$-B. *J. Vac. Sci. Technol. A* **16,** 1934–1937 (1998).
17. Hao, Y. *et al.* Periodically twinned nanowires and polytypic nanobelts of ZnS: The role of mass diffusion in vapor-liquid-solid growth. *Nano Lett.* **6,** 1650–1655 (2006).
18. Akiyama, T. *et al.* An empirical potential approach to wurtzite-zinc-blende polytypism in group III–V semiconducting nanowires. *Jpn. J. Appl. Phys.* **45,** L275–L278 (2006).
19. Glas, F. *et al.* Why does wurtzite form in nanowires of III–V zinc blende semiconductors? *Phys. Rev. Lett.* **99,** 146101 (2007).
20. Minot, E. D. *et al.* Single quantum dot nanowire LEDs. *Nano Lett.* **7,** 367–371 (2007).
21. Malina, V. *et al.* Effect of deposition parameters in the electrical and metallurgical properties of Au-Zn contacts to p-type InP. *Semicond. Sci. Technol.* **9,** 1523–1528 (1994).
22. Weizer, G. W. *et al. Au/Zn Contacts to ρ-InP: Electrical and Metallurgical Characteristics and the Relationship Between Them* (NASA Technical Memorandum 106590, 1994).
23. Brakke, K. E. The surface evolver. *Exp. Math.* **1,** 141–165 (1992).
24. Brakke, K. E. The Surface Evolver Version 2.30. ⟨http://www.susqu.edu/brakke/evolver/evolver.html⟩ (2008).
25. Ross, F. M. *et al.* Sawtooth faceting in silicon nanowires. *Phys. Rev. Lett.* **95,** 146104 (2005).
26. Hurle, D. T. J. A mechanism for twin formation during Czochralski and encapsulated vertical Bridgman growth of III–V compound semiconductors. *J. Cryst. Growth* **147,** 239–250 (1995).
27. Liu, Q. K. K. *et al.* Equilibrium shapes and energies of coherent strained InP islands. *Phys. Rev. B* **60,** 17008 (1999).

Supplementary Information is linked to the online version of the paper at www.nature.com/nature.

Acknowledgements This research was carried out under project number MC3.05243 in the framework of the strategic research programme of the Materials Innovation Institute (M2i), the former Netherlands Institute of Metals Research, the FP6 NODE (015783) project, the Ministry of Economic Affairs in the Netherlands (NanoNed) and the European Marie Curie programme. We thank H. de Barse and F. Holthuysen for SEM imaging and P. van der Sluis, H. Wondergem and M. Decré for discussions.

Author Contributions All authors contributed to the design of experiments. G.I. was responsible for MOVPE growth, and M.A.V. for the TEM experiments. R.E.A. and M.A.V. analysed the TEM data. L.-F.F. and W.J.P.v.E. analysed the data quantitatively. R.E.A., L.-F.F., W.J.P.v.E. and E.P.A.M.B. co-wrote the paper.

Author Information Reprints and permissions information is available at www.nature.com/reprints. Correspondence and requests for materials should be addressed to E.P.A.M.B. (erik.bakkers@philips.com).